Nanostructured manganese oxide clusters supported on mesoporous silica as efficient oxygen-evolving catalysts†

Feng Jiao and Heinz Frei*

Received (in Berkeley, CA, USA) 20th October 2009, Accepted 11th March 2010
First published as an Advance Article on the web 29th March 2010
DOI: 10.1039/b921820c

Nanostructured Mn oxide clusters supported on mesoporous silica KIT-6 efficiently evolve O_2 in aqueous solution under mild conditions.

Generation of a solar fuel on a terawatt scale requires that water is used as electron source.[1] Catalysts for the four-electron oxidation of water to oxygen need not only to fulfill the rate and size requirements for keeping up with the solar flux, but must be robust and made of earth abundant elements. Benefiting from explorations of first row transition metal oxides as O_2 evolving electrocatalysts[2,3] and, in a few cases, chemically driven catalysts[4] over the past several decades, progress on Co oxide-based water oxidation catalysts has recently been reported on two fronts. Nocera's group has employed electrodeposition of Co-containing films on an indium tin oxide anode from an aqueous Co phosphate solution and achieved O_2 evolution at neutral pH and with modest overpotential (10 mA current, 100 percent Faradaic efficiency, 410 mV overpotential).[5] In another direction, a nanostructured silica support has enabled the synthesis of nanometer-sized Co_3O_4 (spinel) clusters which possess a very high surface area (bundles of nanorods of 8 nm diameter). Using a standard visible light sensitizer method for driving the catalyst,[6] we have achieved a turnover frequency (TOF) of 1140 s^{-1} per nanocluster catalyst (pH 5.8, RT, 350 mV overpotential). Projected on a plane, this corresponds to a TOF of 1 s^{-1} nm^{-2}.[7] Therefore, a hundred such nanocluster catalysts stacked in a nanoporous scaffold, which can readily be achieved, will result in a TOF of 100 s^{-1} nm^{-2}, the rate required for keeping up with the solar flux (1000 W m^{-2}, AM 1.5). The high TOF of the Co_3O_4 nanoclusters is mainly attributed to the very high surface area afforded by the nanorod structure, and the high activity of Co surface centers due to the sharply curved nanorod surface.[7] A recent detailed study by Tilley and Bell *et al.* of the size-dependence of the catalytic water oxidation activity for cubic Co_3O_4 nanoparticles (range 5 to 50 nm) loaded on Ni foam anodes in alkaline aqueous solution showed a clear, linear dependence of surface area thus confirming the surface size effect.[8]

In light of the fact that Mn is not only earth abundant but also environmentally friendly, this metal is particularly attractive for use as a catalyst material. In fact, electrochemists have conducted extensive studies on the use of Mn oxides as anode coatings for catalytic O_2 evolution from water.[2,3] While work was typically conducted under basic conditions around pH 14 to minimize the overvoltage, Tamura *et al.* studied water oxidation over a wide range of pH values including neutral aqueous solution for which they reported current densities around 100 mA cm^{-2} corresponding to a TOF of ≥ 0.013 s^{-1} at an overvoltage of 440 mV[2] (the TOF is a lower limit because no BET surface area was reported; therefore, the estimate assumes that all deposited Mn centers are catalytically active[7]). Also under mild conditions (pH 5), Harriman *et al.* demonstrated oxygen evolution in aqueous suspensions of μm-sized Mn_2O_3 particles using photochemically generated $Ru^{3+}(bpy)_3$ as oxidant for driving the catalyst.[4] Taken together, these literature reports suggest that Mn oxides hold promise for developing robust, efficient water oxidation catalysts that can be operated under mild pH and temperature conditions if nano-sized clusters with high surface area can be made. Here we report efficient O_2 evolution at nanostructured Mn oxide clusters in mesoporous silica under very mild conditions for the first time. For driving the catalyst with visible light, the established $Ru^{+2}(bpy)_3$–persulfate sensitizer system was used.[4]

Transmission electron microscopic (TEM) images of Mn oxide nanoclusters synthesized in KIT-6 silica material at 8.0 ± 0.3% loading (per ICP-MS) by wet impregnation followed by controlled calcination are shown in Fig. 1.[9]† By examining many KIT-6 particles (3D network of 8 nm channels), we confirmed that Mn oxide clusters are exclusively formed inside the silica host and do not disrupt the cubic mesopore structure. The latter conclusion is further supported

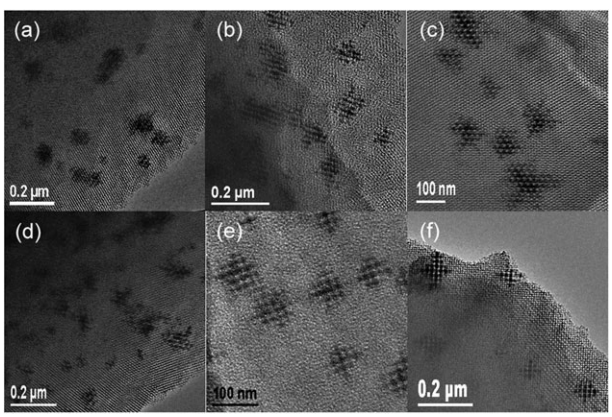

Fig. 1 TEM images for Mn oxide nanoclusters supported on mesoporous silica KIT-6. Calcination treatment: (a) 400 °C, (b) 500 °C, (c) 600 °C, (d) 700 °C, (e) 800 °C, (f) 900 °C.

Physical Biosciences Division, Lawrence Berkeley National Laboratory, University of California, Berkeley, CA 94720, USA. E-mail: hmfrei@lbl.gov; Tel: +1-510-486-4325
† Electronic supplementary information (ESI) available: Synthesis details, low angle PXRD results, particle size analysis, and wide angle PXRD patterns. See DOI: 10.1039/b921820c

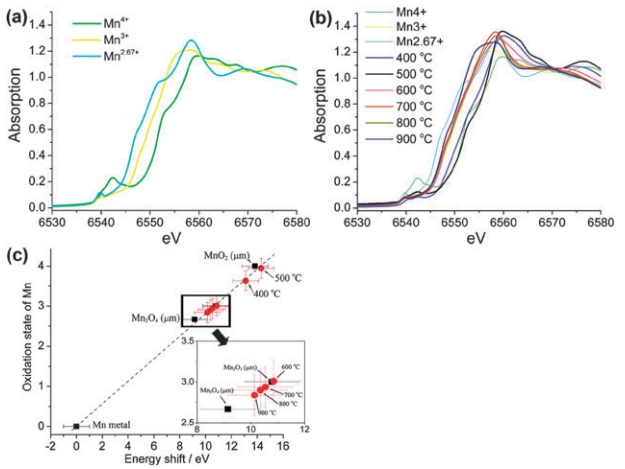

Fig. 2 X-Ray absorption measurements of KIT-6/MnO_x samples and reference Mn oxide materials. (a) XANES spectra of micron-sized particles of MnO_2 (blue), Mn_2O_3 (yellow), and Mn_3O_4 (green). (b) XANES spectra of KIT-6/Mn oxide materials calcined at temperatures between 400 and 900 °C. To facilitate comparison, traces of the reference materials of panel (a) are also shown in faint color. (c) Average oxidation state of Mn for the various KIT-6/Mn oxide samples derived from the K-edge energy.

by low angle XRD measurements, shown in Fig. S1, ESI†, which exhibit strong [211], [220], and [332] diffraction peaks (*Ia3d* space group of KIT-6).† The approx. spherical clusters, which replicate the pore structure of the silica support, have mean diameters in the range 73–86 nm depending on the calcination temperature, with narrow size distributions throughout (Table S1 and Fig. S2, ESI†). On the other hand, only a single diffraction peak was observed in the wide angle powder XRD spectra (Fig. S3, ESI†), and only for samples calcined at 700 °C and above, which is attributed to the α-Mn_2O_3 phase.† The absence of other peaks indicates that the crystal domain sizes are too small for detection by powder XRD, or that the Mn oxide clusters are amorphous.

Mn K-edge X-ray absorption spectroscopy was carried out to obtain more detailed information on the atomic structure of the Mn oxide clusters. As can been seen from the X-ray absorption near edge structure (XANES) spectra of Mn oxide/KIT-6 materials in Fig. 2b, the K-edge position depends on the calcination temperature. For comparison, edge spectra of standard manganese oxide particles (μm size) of MnO_2, Mn_2O_3, and Mn_3O_4 are displayed in Fig. 2a. It is well established that the K-edge shifts to higher energies with increasing Mn oxidation state. Exploiting the established linear relationship between K-edge energy and Mn oxidation state, the mean oxidation state of the metal can be determined, as shown in Fig. 2c. According to this plot, materials calcined at 500 °C feature mainly Mn^{+4}, while the mean Mn oxidation state decreases gradually towards higher calcination temperature, from Mn^{+3} at 600 °C (corresponding to Mn_2O_3) to $Mn^{+2.85}$ for the sample calcined at 900 °C. A more quantitative understanding of structural composition of the Mn oxide clusters was obtained by a computer-based component analysis study of the XANES spectra using a least squares fitting program of the software package SIXPACK (S. Webb, SSRL, Stanford). The analysis provided the fractional composition of the KIT-6/Mn oxide catalyst for each calcination temperature. The results, summarized in Table S2, ESI†, indicate that the contribution of MnO_2 reaches a maximum at 500 °C while that of the spinel phase (Mn_3O_4) contributes significantly only above 600 °C and then increasingly so towards higher temperatures. The Mn_2O_3 phase, on the other hand, is dominant between 600 and 700 °C, and then declines. XANES spectra of μm-sized β-MnO_2, α-Mn_2O_3, and Mn_3O_4 particles were used for Mn K-edge fitting. Hence, increase of the calcination temperature reduces Mn^{+4} to Mn^{+3} and, above 700 °C, partially to Mn^{+2}. As will be shown below, the material calcined at 600 °C is of most interest from a catalyst activity standpoint, and its main phase is Mn_2O_3. We conclude from the X-ray absorption, XRD and TEM analyses that spherically shaped, mixed-phase Mn oxide nanoclusters of 70–90 nm diameter are obtained in mesoporous KIT-6 silica scaffolds, with MnO_2, Mn_2O_3 and Mn_3O_4 in varying amounts as main components.

Visible light-driven O_2 evolution in aqueous suspensions of Mn oxide/KIT-6 catalysts was determined by mass spectrometric analysis of the gas in the head space volume according to the detailed description in the ESI†. The 40 mL buffered solution (Na_2SiF_6, $NaHCO_3$, 0.022–0.028 M, pH 5.8) contained 130 mg $Na_2S_2O_8$ (electron acceptor), 390 mg Na_2SO_4, 45 mg ($[Ru(bpy)_3]Cl_2 \cdot 6H_2O$ (sensitizer), and 200 mg Mn oxide/KIT-6 (8%, containing 12 mg Mn). For experiments with μm-sized Mn oxide particles, 200 mg of MnO_2, Mn_2O_3, or Mn_3O_4 were used. Mildly acidic conditions were used in order to minimize photodegradation of the Ru sensitizer[10] (while an established sensitizer for driving various types of water oxidation catalysts and comparing their rates, $Ru(bpy)_3$ is too unstable for use in practical systems). For all catalyst samples, the amount of O_2 generated increased close to linearly over the initial 30 min of photolysis but leveled off after about one hour because of consumption of persulfate acceptor. This was confirmed by adding another 130 mg of NaS_2O_8 to the photolysed solution, re-adjusting the pH from 5.08 to 5.80 with $NaHCO_3$ and bubbling Ar for 30 min to remove any dissolved O_2, and continuing photolysis under identical conditions. Within experimental error of 5%, the same O_2 yield was measured as in the initial run demonstrating the stability of the Mn oxide/KIT-6 catalyst. Recording of the K-edge position by X-ray absorption spectroscopy of the Mn oxide/KIT-6 catalysts before and after photolysis confirmed the integrity of the Mn oxidation state.

A series of control experiments was conducted to test for possible alternative sources of water oxidation activity. No O_2 evolution was detected when conducting a photolysis experiment with an aqueous solution containing 25 μg L^{-1} Mn^{+2}. This corresponds to the concentration of Mn^{+2} in the solution detected by ICP-MS after a photolysis experiment with Mn oxide/KIT-6 (600 °C). The result confirms that the very small fraction of Mn ions (4×10^{-7}) leaching into solution is not responsible for water oxidation catalysis. Furthermore, catalytic activity of any decomposition products of the $Ru^{+2}(bpy)_3$ sensitizer was ruled out by the lack of O_2 generation when conducting the photolysis experiment in the presence of sensitizer and plain (Mn oxide-free) KIT-6 powder. In this case, the sensitizer deteriorates rapidly, but no O_2 from decomposition products was detected.

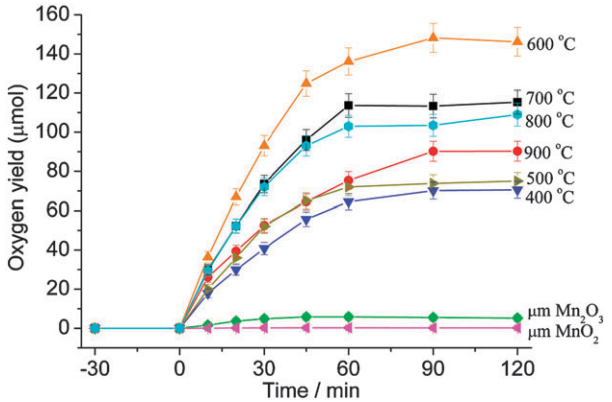

Fig. 3 Oxygen evolution in aqueous suspension (40 mL) of KIT-6/Mn oxide using the $Ru^{2+}(bpy)_3$–persulfate visible light sensitization system (476 nm, 240 mW), conducted at pH 5.8 and 22 °C.

From the amount of O_2 gas evolved during the initial 10 min of photolysis for each Mn oxide/KIT-6 material (Fig. 3), taking into account the equilibrium oxygen concentration in the solution volume,[11] the turnover frequency per Mn oxide nanocluster was estimated. The calculation is based on the geometry of the cluster (mean diameter of sphere, Table S1, ESI†), the loading of 16 mg Mn oxide, the average density of the cluster taking into account its composition (Table S2, ESI†) and density of individual phases, and the pore volume taken up by the Mn oxide material inside the KIT-6 pores.† We obtain TOF = 1630 s^{-1} per Mn oxide nanocluster for Mn oxide/KIT-6 calcined at 400 °C, 1210 s^{-1} (500 °C), 3330 s^{-1} (600 °C), 1260 s^{-1} (700 °C), 1590 s^{-1} (800 °C), 1830 s^{-1} (900 °C). The TOF was not limited by the intensity of the visible light used to excite the sensitizer and is therefore an intrinsic property of the Mn oxide catalyst. The catalyst prepared by calcination at 600 °C has the highest activity. This material contains a high content of Mn_2O_3 (Table S2, ESI†); previous electrocatalytic studies also revealed that Mn trioxide anode coatings were the most efficient for water oxidation.[3]

A useful figure of merit for solar photocatalytic applications is the TOF per area when the catalyst is projected onto a plane, which for this catalyst is 0.6 s^{-1} nm^{-2}, close to 1 s^{-1} nm^{-2} of Co_3O_4 nanoclusters in SBA-15.[7] Therefore, stacking of between one and two hundred Mn oxide nanoclusters in the mesoporous silica scaffold will allow the ensemble of nanocluster catalysts to keep up with the solar flux. In addition to offering an approach for achieving the required turnover frequency per unit area, arranging the nanoclusters in a silica scaffold assures a perfect, stable dispersion of the catalysts, which is critical for maximizing activity. Mixed phase Mn oxide nanoclusters inside KIT-6 silica scaffolds are competent catalysts for O_2 evolution from water operating under mild pH conditions at RT and at modest overpotential of 350 mV ($\varepsilon^o(Ru^{+3}(bpy)_3/Ru^{+2}(bpy)_3$ = 1.24 V, $\varepsilon^o(O_2/H_2O)$ = 0.89 V at pH 5.6).[7]

As can be seen from Fig. 3, the oxygen yield is 26 times smaller for an aqueous suspension of 16 mg of bare μm Mn_2O_3 particles (containing 11.1 mg Mn) compared to that of the nanoclusters of Mn oxide/KIT-6 (600 °C) (containing 12 mg Mn). The result confirms that the interior of the particles or clusters is not involved in the catalysis.

In conclusion, nanometer-sized Mn oxide clusters supported on a mesoporous silica scaffold have been established as efficient water oxidation catalysts in aqueous solution at RT and pH 5.8. The high surface area silica support may be critical for the integrity of the catalytic system by offering a perfect, stable dispersion of the nanostructured Mn oxide clusters. In addition, it is likely that the silica environment plays an important role for sustaining activity by protecting the active Mn centers of the catalyst from deactivation by surface restructuring. Moreover, the mesoporous support offers a method for the stacking of catalytic particles to achieve turnover rates per projected geometrical area that are adequate for keeping up with the solar flux.

This work was funded by the Helios Solar Energy Research Center, which is supported by the Director, Office of Science, Office of Basic Energy Sciences of the U.S. Department of Energy under Contract No. DE-AC02-05CH11231. The authors acknowledge the support of the National Center for Electron Microscopy, Lawrence Berkeley National Laboratory, which is supported by the U.S. Department of Energy. Portions of this research were carried out at the Stanford Synchrotron Radiation Laboratory, a national user facility operated by Stanford University on behalf of the U.S. Department of Energy, Office of Basic Energy Sciences.

Notes and references

1 N. S. Lewis and D. G. Nocera, *Proc. Natl. Acad. Sci. U. S. A.*, 2006, **103**, 15729.
2 M. Morita, C. Iwakura and H. Tamura, *Electrochim. Acta*, 1977, **22**, 325.
3 M. Morita, C. Iwakura and H. Tamura, *Electrochim. Acta*, 1978, **23**, 331; M. Morita, C. Iwakura and H. Tamura, *Electrochim. Acta*, 1979, **24**, 357; R. Mraz, V. Srb and S. Tichy, *Electrochim. Acta*, 1973, **18**, 551; Y. Matsumoto and E. Sato, *Electrochim. Acta*, 1979, **24**, 421; Y. Matsumoto and E. Sato, *Mater. Chem. Phys.*, 1986, **14**, 397; K. Fujimura, T. Matsui, K. Izumiya, N. Kumagai, E. Akiyama, H. Habazaki, A. Kawashima, K. Asami and K. Hashimoto, *Mater. Sci. Eng., A*, 1999, **267**, 254; M. S. El-Deab, M. I. Awad, A. M. Mohammad and T. Ohsaka, *Electrochem. Commun.*, 2007, **9**, 2082.
4 A. Harriman, I. J. Pickering, J. M. Thomas and P. A. Christensen, *J. Chem. Soc., Faraday Trans. 1*, 1988, **84**, 2795.
5 M. W. Kanan and D. G. Nocera, *Science*, 2008, **321**, 1072; Y. Surendranath, M. Dinca and D. G. Nocera, *J. Am. Chem. Soc.*, 2009, **131**, 2615.
6 P. Huang, A. Magnuson, R. Lomoth, M. Abrahamsson, M. Tamm, L. Sun, B. van Rotterdam, J. Park, L. Hammarstrom, B. Akermark and S. Styring, *J. Inorg. Biochem.*, 2002, **91**, 159; W. J. Youngblood, S. H. A. Lee, Y. Kobayashi, E. A. Hernandez-Pagan, P. G. Hoertz, T. A. Moore, A. L. Moore, D. Gust and T. E. Mallouk, *J. Am. Chem. Soc.*, 2009, **131**, 926.
7 F. Jiao and H. Frei, *Angew. Chem., Int. Ed.*, 2009, **48**, 1841.
8 A. J. Esswein, M. J. McMurdo, P. N. Ross, A. T. Bell and T. D. Tilley, *J. Phys. Chem. C*, 2009, **113**, 15068.
9 F. Jiao and P. G. Bruce, *Adv. Mater.*, 2007, **19**, 657.
10 M. Hara, C. C. Waraksa, J. T. Lean, B. A. Lewis and T. E. Mallouk, *J. Phys. Chem. A*, 2000, **104**, 5275.
11 H. Han and H. Frei, *J. Phys. Chem. C*, 2008, **112**, 16156.

